ISSN 1062-8738, Bulletin of the Russian Academy of Sciences: Physics, 2017, Vol. 81, No. 10, pp. 1230–1238. © Allerton Press, Inc., 2017.

A Novel Method for Determining the Single Particle Potential Directly from the Measured Single Particle Density: Application to the Charge Density Difference between the Isotones ^{206}Pb –^{205}Tl[1]

S. Shlomo[a, b, *] and M. R. Anders[b]

[a]*Cyclotron Institute, Texas A&M University, College Station 77840, Texas, USA*
[b]*The Weizmann Institute of Science, 234 Herzl St., PO Box 26, Rehovot, 7610001 Israel*
**e-mail: s-shlomo@tamu.edu*

Abstract—We present a novel method, based on the single particle Schroedinger equation, to determine the central potential (mean-field) directly from the single particle matter density and its first and second derivatives. As an example, we consider the experimental data for the charge density difference between the isotones ^{206}Pb –^{205}Tl, deduced by phase shift analysis of elastic electron scattering cross-section measurements and corresponds to the shell model $3s_{1/2}$ proton orbit, and determine the corresponding single particle potential. We also present results of least-square fits to parametrized single particle potentials. The $3s_{1/2}$ wave functions of the determined potentials reproduce fairly well the experimental data within the quoted errors. More accurate experimental data, with uncertainty smaller by a factor of two or more, may answer the question how well can the data be reproduced by a calculated $3s_{1/2}$ wave function.

DOI: 10.3103/S1062873817100227

INTRODUCTION

The nuclear shell model is based on the assumption that nucleons in the atomic nucleus move independently in single particle orbits in a common potential well (mean-field). As well known, it has been very successful in explaining many features of nuclei [1]. In determining the nuclear mean-field potential, it is common to: (i) parametrize the central potential, using for example, the Woods–Saxon form. The parameters are determined by a fit of calculated properties, such as single particle energies and reaction cross-sections, to the corresponding experimental data [2]; and (ii) by carrying out Hartree–Fock calculations using a parametrized effective two-body interaction. The parameters are determined by a fit to experimental data, such as binding energies and nuclear radii [3]. In this work we present a novel method, based on the single particle Schroedinger equation for a wave function $\Psi(\vec{r})$ with eigenenergy E, to determine the central potential $V(\vec{r})$ directly from the measured single particle matter density, $\rho(\vec{r}) = [\Psi(\vec{r})]^2$ and its second derivatives, assuming that they are known for all $(\vec{r})$.

[1] The article is published in the original.

The relation between shell model wave functions and the real nuclear ones is rather complicated. Important information about it may be gleaned from the measurement of the charge distribution of the proton $3s_{1/2}$ orbit. This is given by the measured charge density difference, $\Delta\rho_c(r)$, between charge density distributions of the isotones ^{206}Pb – ^{205}Tl. This difference was determined many years ago, by analysis of elastic electron scattering measurements [4, 5]. The experimental data of the charge density shows a clear maximum at the center of ^{206}Pb with two additional maxima. This seems to be the shape obtained from a $3s_{1/2}$ single proton wave-function, in agreement with the simple shell model. It was pointed out [4] that commonly used central potentials, such as the Woods–Saxon potential, lead to a $3s_{1/2}$ charge density in disagreement with experimental data. In particular, the central density obtained from the Woods–Saxon potential is too large by 40%.

This difference between data and the Woods–Saxon results was considered in Ref. [6]. In that paper, it seems that it is consistent with effects of two-body short range correlations on the shell model wave functions. Using our new method, we look in this work for

a single particle nuclear potential whose proton $3s_{1/2}$ orbit yields a charge distribution which reproduces the experimental one. The resulting single particle potential, if found, will provide a stringent limit on the effects of short range correlations on the expected values of long-range operators. The potential can also be used as an additional experimental constraint in determining a modern energy density functional (EDF), needed for more reliable prediction of properties of nuclei and nuclear matter [3, 7]. A summary of the results of the present work were publishes in Refs. [8, 9]. Here, a detailed derivation of the novel method is presented, as well as a detailed description of the search for a potential well which will yield a good fit to the ^{206}Pb–^{205}Tl experimental data.

In section II we consider the single particle Schroedinger equation and describe the method for determining the single particle potential $V(\vec{r})$ from a given single particle wave function $\Psi(\vec{r})$ or matter density, $\rho(\vec{r}) = [\Psi(\vec{r})]^2$, assuming it is known for all $\vec{r}$ [1]. In particular, we consider the case of spherical symmetry. We also describe the method of deducing the point proton density from the charge distribution determined in electron scattering measurement. In section III we present results for the case of the experimental data [4, 5] for the charge density difference between the close ($\Delta Z = 1$) isotones ^{206}Pb–^{205}Tl, associated with the $3s_{1/2}$ proton single particle orbit, and determine the corresponding single particle potential. In Section IV we present our conclusions.

1. FORMALISM

1.1. Determining Single Particle Potential from Single Particle Matter Density

Consider the single particle Schroedinger equation,

$$-\frac{\hbar^2}{2m}\Delta\Psi + V\Psi = E\Psi, \tag{1}$$

where $V(\vec{r})$ is a real local and non-singular potential and $\Delta = (\vec{\nabla},\vec{\nabla})$, with $\vec{\nabla}$ being the gradient operator. For a given single particle wave function $\Psi(\vec{r})$, known for all $(\vec{r})$, and given eigenvalue E, we obtain from Eq. (1) that the corresponding single particle potential V is uniquely determined [1] from

$$V(\vec{r}) = E + \frac{\hbar^2}{2m}S(\vec{r}),\ \ S(\vec{r}) = \frac{\Delta\Psi(\vec{r})}{\Psi(\vec{r})}. \tag{2}$$

We note that for a nonsingular V, $\Delta\Psi(\vec{r}) = 0$ when $\Psi(\vec{r}) = 0$. It is important to point out that in the analysis of experiments, such as electron scattering, one determines the matter density $\rho(\vec{r}) = [\Psi(\vec{r})]^2$, for real Ψ. Operating with Δ on $[\Psi(\vec{r})]^b$, where b is positive and real, and using the relation $\vec{\nabla}\Psi^b = b\Psi^{b-1}\vec{\nabla}\Psi$ with the definition $S(\vec{r}) = \dfrac{\Delta\Psi(\boldsymbol{r})}{\Psi(\boldsymbol{r})}$ of Eq. (2), we obtain the general relation

$$S(\vec{r}) = \frac{\Delta[\Psi(\vec{r})]^b}{b[\Psi(\vec{r})]^b} - \frac{b-1}{b^2}\left[\frac{\vec{\nabla}[\Psi(\vec{r})]^b}{[\Psi(\vec{r})]^b}\right]^2. \tag{3}$$

Note that Eq. (2) is a special case of Eq. (3) for $b = 1$. For $b > 2$, $\vec{\nabla}[\Psi(\vec{r})]^b = 0$ and $\Delta[\Psi(\vec{r})]^b = 0$ when $[\Psi(\vec{r})]^b = 0$. For $b = 2$, we have from Eqs. (2) and (3) that the potential $V(\vec{r})$ is given in term of the corresponding single particle matter density $\rho(\vec{r})$ (for real $\Psi(\vec{r})$) and its first and second derivatives.

In the spherical case the wave function of a nucleon is written as

$$\Psi_{nlj}(\vec{r}) = \frac{R_{nlj}(r)}{r}Y_{lj}, \tag{4}$$

where $R_{nlj}(r)$ is the (one-dimensional) radial wave function for the orbit with principle number n, orbital angular momentum l and total angular momentum j and Y_{lj} is the known spin harmonic wave function, with the normalization

$$\int R_{nlj}^2(r)\,dr = 1. \tag{5}$$

The corresponding single particle potential for a nucleon has the form

$$\begin{aligned} V(r) = V_{\rm cen}(r) + (\vec{s},\vec{l})V_{\rm s.o.}(r) \\ + \frac{1}{2}(1-\tau_z)V_{\rm coul}(r), \end{aligned} \tag{6}$$

where $V_{\rm cen}(r), (\vec{s},\vec{l})V_{\rm s.o.}(r)$ and $\frac{1}{2}(1-\tau_z)V_{\rm coul}(r)$, are the nuclear central, spin-orbit and Coulomb potentials, respectively, and $\tau_z = 1$ for a neutron and -1 for a proton. Using Eqs. (2), (4) and (6) we have that nuclear central potential is given by,

$$\begin{aligned} V_{\rm cen}(r) = E + \frac{\hbar^2}{2m}S(r) - \frac{\hbar^2}{2m}\frac{l(l+1)}{r^2} \\ - \frac{1}{2}(1-\tau_z)V^{\rm coul}(r) - c_{ls}V_{\rm s.o.}(r), \end{aligned} \tag{7}$$

$$S(r) = \frac{d^2R_{nlj}}{dr^2}\frac{1}{R_{nlj}(r)}.$$

where $c_{ls} = -l(l+1)$ and l for $j = l - 1/2$ and $j = l + 1/2$, respectively. The single particle radial density $\rho_{nlj}(r)$ is related to the square of the single particle radial wave function R_{nlj}^2 by

$$R_{nlj}^2(r) = 4\pi r^2\rho_{nlj}(r). \tag{8}$$

Using Eq. (1) one can deduce the radial wave-function $R_{nlj}(r)$ and determine the central potential using Eq. (7). But this leads to numerical complication, particularly in the vicinity of the nodes of the wave function. From Eq. (1) for the radial wave-function $R_{nlj}(r)$ and Eq. (3) for $b = 2$ we have that the corresponding single particle potential V can be obtained from (6) by using the simple relation

$$S(r) = \frac{1}{2R_{nlj}^2}\left[\frac{d^2\left(R_{nlj}^2\right)}{dr^2} - \frac{1}{2}\left[\frac{1}{R_{nlj}}\frac{d\left(R_{nlj}^2\right)}{dr}\right]^2\right]. \quad (9)$$

From Eqs. (8) and (9) we find the relation

$$S(r) = \frac{1}{2\rho_{nlj}} \times \left[\frac{d^2\rho_{nlj}}{dr^2} + \frac{2}{r}\frac{d\rho_{nlj}}{dr} - \frac{1}{2\rho_{nlj}}\left(\frac{d\rho_{nlj}}{dr}\right)^2\right]. \quad (10)$$

Equation (10) can also be derived from Eq. (3) with $b = 2$ using the (real) three-dimensional wave function and the operators Δ and $\vec{\nabla}$ in spherical coordinates.

As an example we note that for the single particle radial wave function of the form $R \sim \sin(kr + \varphi)$, an eigenstate of a constant potential, one finds from (7) the corresponding constant potential $V = E - \frac{\hbar^2 k^2}{2m}$. Similarly, for the Harmonic Oscillator $3s_{1/2}$ single particle wave function

$$R_{3s/2}(r) = \left(\frac{15}{2\sqrt{\pi}}\nu^{3/2}\right)^{1/2} re^{-\frac{1}{2}\nu r^2} \times \left[1 - \frac{4}{3}\nu r^2 + \frac{4}{15}\left(\nu r^2\right)^2\right], \quad (11)$$

with the size parameter $\nu = \frac{m\omega}{\hbar}$ we have from (7) the expected potential

$$V(r) = E - \frac{11}{2}\hbar\omega + \frac{1}{2}m\omega^2 r^2, \quad (12)$$

We note that for the central nuclear potential it is common to use the Woods Saxon (WS) form,

$$V(r) = V_0/\left[1 + \exp\left((r - R_1)/a_0\right)\right], \quad (13)$$

where, V_0, R_1 and a_0 are the depth, half radius and diffuseness parameters, respectively. Furthermore, for the Coulomb potential we adopt the form obtained from a uniform charge distribution of radius $R_{\rm ch}$,

$$V^{\rm coul}(r) = Ze^2\begin{cases}(3 - r^2/R_{\rm ch}^2)/2R_{\rm ch} & r < R_{\rm ch}\\ 1/r & r > R_{\rm ch}\end{cases}, \quad (14)$$

In Eqs. (14), $R_{\rm ch}$ is the equivalent radius determined by the charge root-mean-square radius, $r_{\rm ch}^2$

$$R_{\rm ch}^2 = (5/3)r_{\rm ch}^2. \quad (15)$$

The form of the spin-orbit potential is commonly taken as,

$$V_{\rm s.o.}(r) = cdV_{\rm cen.}(r)/dr, \quad (16)$$

where c is adjusted to the experimental spin-orbit splittings (~ 0.2).

1.2. Determining the Point Proton Density from the Charge Density

In elastic electron-nucleus scattering measurement one determines the charge density distribution, $\rho_c(\vec{r})$, by carrying out a phase shift analysis of the cross section [10], whereas in theoretical model one calculates the point proton density distribution, $\rho_p(\vec{r})$. They are related by,

$$\rho_c(\vec{r}) = \int \rho_p(\vec{r}\,')\rho_{pfs}(\vec{r} - \vec{r}\,')d\vec{r}\,', \quad (17)$$

where $\rho_{pfs}(\vec{r})$ is the charge density distribution of a free proton. From elastic electron scattering on a free proton one finds that,

$$\rho_{pfs}(\vec{r}) = \frac{1}{8\pi a^3}e^{-r/a}, \quad (18)$$

where $a^2 = \frac{1}{12}r_{pfs}^2$ with $r_{pfs} = 0.85$ fm being the corresponding charge root mean square (rms) radius. The charge mean square radius is given by

$$r_c^2 = \int r^2\rho_c(\vec{r})\,d\vec{r}\Big/\int \rho_c(\vec{r})\,d\vec{r}. \quad (19)$$

From Eqs. (17) and (19) one has the relation

$$r_c^2 = r_p^2 + r_{pfs}^2. \quad (20)$$

Considering below the spherical case, we have using Eqs. (17) and (18), that

$$\rho_c(\vec{r}) = \frac{1}{4\pi a}\int_0^\infty r'\,dr'\,\rho_p(r') \times \left[\left(1 + \frac{|r - r'|}{a}\right)e^{-|r-r'|/a} - \left(1 + \frac{(r + r')}{a}\right)e^{-(r+r')/a}\right]. \quad (21)$$

It is common [8] to define the form factor $F(q)$ as the Fourier transform of the density $\rho(r)$ as

$$F(q) = \frac{4\pi}{q}\int_0^\infty \sin(qr)\rho(r)rdr. \quad (22)$$

The corresponding inverse transform is given by

$$\rho(r) = \frac{1}{(2\pi)^3}\frac{4\pi}{r}\int_0^\infty \sin(qr)F(q)qdq. \quad (23)$$

For the proton charge distribution of Eq. (18) we have the dipole form

$$F_{pfs}(q) = \left(1 + \frac{1}{12} r_{pfs}^2 q^2\right)^{-2}. \quad (24)$$

For the charge density $\rho_c(r)$, given by the convolution relation of Eq. (17) we have the simple relation for the form factors

$$F_c(q) = F_{pfs}(q) F_p(q). \quad (25)$$

Eq. (25) can be used to determine the form factor $F_p(q)$, associated with the point proton density distribution $\rho_p(r)$, Eq. (17). Then $\rho_p(r)$ can be obtained from $F_p(q)$, using (23) and compared with theoretical predictions.

2. RESULTS

In this work we consider the charge density difference,

$$\Delta\rho_c(r) = \rho_c(r;\ ^{206}\mathrm{Pb}) - \rho_c(r;\ ^{205}\mathrm{Tl}), \quad (26)$$

between the isotones ^{206}Pb – ^{205}Tl, associated with the proton $3s_{1/2}$ single particle orbit, and determine the corresponding single particle potential. The experimental data for the charge densities, $\rho_c(r)$, of the isotones ^{206}Pb and ^{205}Tl, obtained from accurate elastic electron scattering experiments, are taken from Refs. [4, 5], where they are given in term of sums of Gaussian functions of r.

In Fig. 1a we present the experimental data for the charge density difference, $\Delta\rho_c(r)$, between the isotones ^{206}Pb–^{205}Tl, shown by the solid line. It is normalized to a total charge of one proton ($Z = 1$). The experimental uncertainty is indicated by the dotted lines. Note that the two nodes associated with the proton $3s_{1/2}$ orbit are clearly seen in the figure. The experimental values of the charge rms radii of ^{206}Pb and ^{205}Tl are 5.4897 and 5.4792 fm, respectively, leading to a value of 6.2822 fm for the charge rms radius of the proton $3s_{1/2}$ orbit. To determine the corresponding single particle potential, using Eqs. (7) and (9) or (10), the point proton distribution, $\Delta\rho_p(r)$, is needed. This is obtained by using Eqs. (22), (24) and (25) to determine the point proton form factor, $F_p(q)$, and then employing Eq. (23) to obtain $\Delta\rho_p(r)$. The results are shown as a solid line in Fig. 1b. The experimental uncertainty is shown by the dotted lines. Using the value of $r_{pfs} = 0.85$ in Eq. (20), we find that the rms radii of the proton density distributions of ^{206}Pb and ^{205}Tl are 5.4235 and 5.4129 fm, respectively, leading to a value of 6.2244 fm for the rms radius of the point proton $3s_{1/2}$ orbit. Note that $\Delta\rho_p(r)$ (solid line) is slightly negative at the first node ($r \sim 2.6$ fm) and above zero at the second node ($r \sim 4.9$ fm). Moreover,

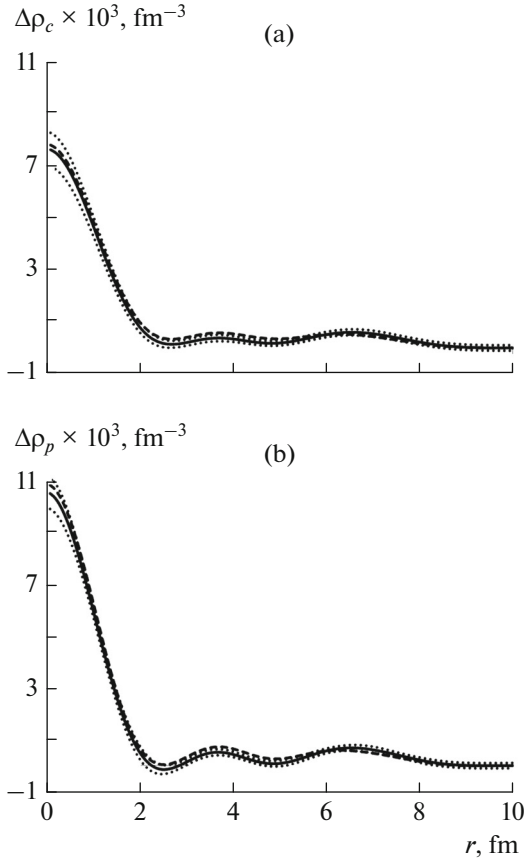

Fig. 1. (a) The experimental difference, $\Delta\rho_c(r)$ between ^{206}Pb and ^{205}Tl charge distributions (solid line). The dashed line is for $\Delta\rho_{Rc}(r)$, the data after rearrangement correction. The dotted lines indicate the experimental uncertainty. (b) The experimental difference, $\Delta\rho_p(r)$ between ^{206}Pb and ^{205}Tl charge distributions (solid line). The dashed line is for $\Delta\rho_{Rp}(r)$, the data after rearrangement correction. The dotted lines indicate the experimental uncertainty.

in the vicinity of these minima, the experimental uncertainty in $\Delta\rho_p(r)$ is larger than its value.

We also present in Figs. 1a, 1b (dashed line) the charge density $\Delta\rho_{Rc}(r)$ and the point particle density $\Delta\rho_{Rp}(r)$ of the proton $3s_{1/2}$ orbit, respectively, corrected for the rearrangement effect (from ^{205}Tl to ^{206}Pb). We adopted the scaling model to assess the rearrangement effect [11]. The charge distribution of ^{205}Tl is scaled so that the charge rms radius of the scaled density is equal to that of the 81 core protons in ^{206}Pb. We obtained,

$$\Delta\rho_{Rc}(r) = \rho_c(r;^{206}\ \mathrm{Pb}) - \alpha^3 \rho_c(\alpha r;\ ^{205}\mathrm{Tl}), \quad (27)$$

where the scaling parameter $\alpha = 5.4792/5.4848 = 0.9990$ is the ratio between the charge rms radius of ^{205}Tl to that of the core 81 protons in ^{206}Pb. The value of 5.4848 fm is obtained by adopting the Harmonic Oscillator approximation for the single particle proton

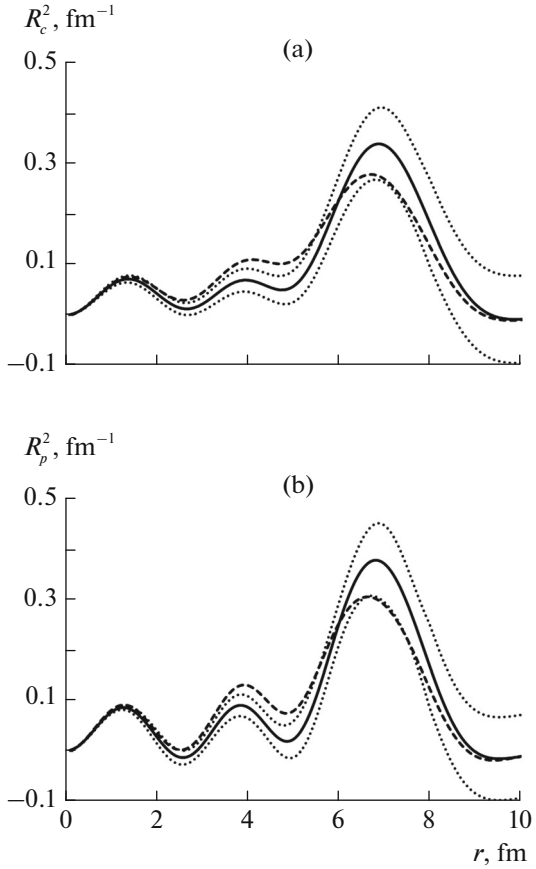

Fig. 2. Similar to Fig. 1. (a) $R_c^2(r) = 4\pi r^2 \Delta\rho_c(r)$. The dashed line is for $R_{Rc}^2(r)$ related to $\Delta\rho_{Rc}(r)$. (b) $R_P^2(r) = 4\pi r^2 \Delta\rho_p(r)$ where $\Delta\rho_p(r)$ is derived from the experimental $\Delta\rho_c(r)$. The dashed line is for $R_{Rp}^2(r)$ related to $\Delta\rho_{Rp}(r)$ similarly obtained from $\Delta\rho_{Rc}(r)$.

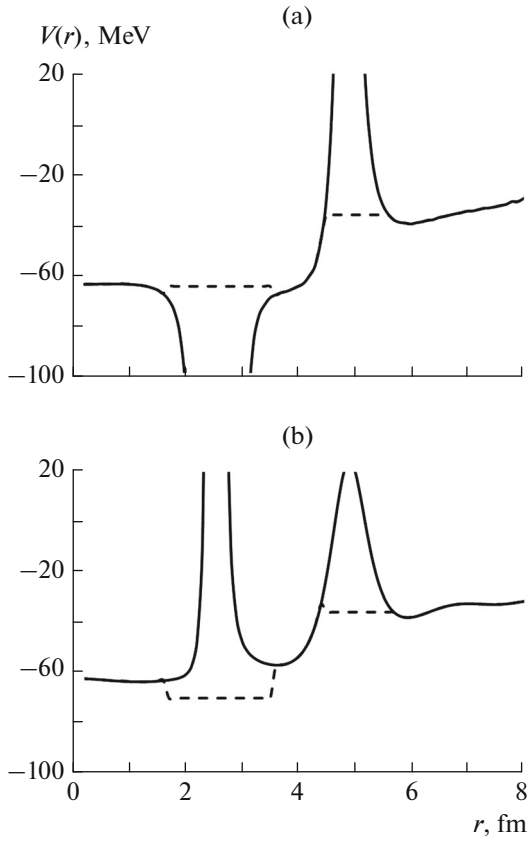

Fig. 3. (a) The solid line is the potential derived from the $R_p^2(r) = 4\pi r^2 \Delta\rho_p(r)$ using Eqs. (7) and (9). The dashed line is the potential derived from an $R_p = A\sin(kr + \varphi)$ fit near each of the minima of $R_p^2(r)$ since the potential blows up. (b) Similar to (a) except rearrangement correction has been taken into consideration.

orbits in ^{206}Pb and subtracting the contribution of the proton $3s_{1/2}$ orbit, using the value of $r_{pfs} = 0.85$ fm. We add that the same value of α is obtained by assuming that the charge rms radius of the core 81 protons in ^{206}Pb is larger than that of ^{205}Tl by 0.005 fm, a value similar to the change in the charge rms radii for isotone in this region [11]. We note that $\Delta\rho_{Rp}(r)$ of Eq. (27) is normalized to 1. It is seen from Fig. 1b that $\Delta\rho_{Rp}(r)$ (dashed line) is above zero at the first node ($r \sim 2.6$ fm) and at the second node ($r \sim 4.9$ fm). We point out that the magnitude of the difference between $\Delta\rho_p(r)$ and $\Delta\rho_{Rp}(r)$ is similar to that of the experimental uncertainty.

Using the relation (8) we determined the corresponding square of the $3s_{1/2}$ convoluted (charge) radial wave function $R_c^2(r) = 4\pi r^2 \Delta\rho_c(r)$ as obtained from Fig. 1a and shown by the solid line in Fig. 2a. Similarly, $R_{Rc}^2(r) = 4\pi r^2 \Delta\rho_{Rc}(r)$, the dashed line in Fig. 2a is obtained from the dashes line in Fig. 1a. The dotted lines indicate the experimental uncertainty. In Fig. 2b we present the square of the point particle radial wave function $R_p^2(r) = 4\pi r^2 \Delta\rho_p(r)$, (solid line) obtained from the solid line of Fig. 1b. The dotted lines indicate the experimental uncertainty. Similarly, $R_{Rp}^2(r) = 4\pi r^2 \Delta\rho_{Rp}(r)$, the dashed line in Fig. 2b is obtained from the dashed line in Fig. 1b.

We have therefore used the experimental $R_p^2(r)$ of Fig. 2b, shown by the solid line, to directly deduce the corresponding potentials by employing Eqs. (6), (7) and (9), obtaining the results shown in Fig. 3a by the solid line. Similarly, in Fig. 3b we show the potential obtained from $R_{Rp}^2(r)$ of Fig. 2b. The Coulomb potential of Eq. (14), with $R_{ch} = 7.1$ fm, was adopted in the calculations. For the $3s_{1/2}$ orbit, there is no contribution from the centrifugal and spin-orbit potentials. We

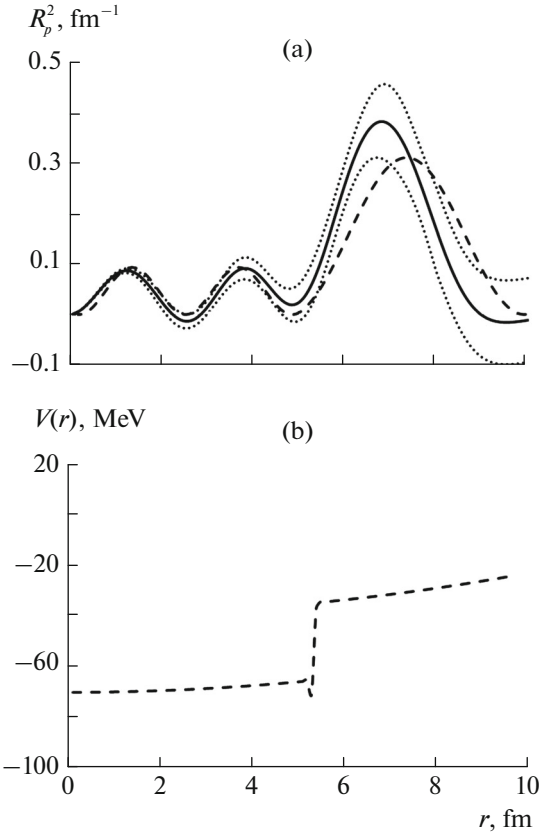

Fig. 4. (a) The experimental difference, $R_p^2(r) = 4\pi r^2 \Delta\rho_p(r)$ between ^{206}Pb and ^{205}Tl charge distributions (solid line). The dashed line is for an $R_p = A\sin(kr + \varphi)$ fit with two separate Sine functions spliced together at $r \sim 5.3$ fm. The dotted lines indicate the experimental uncertainty. (b) The dashed line is the potential derived from the spliced Sine functions, using Eqs. (7) and (9).

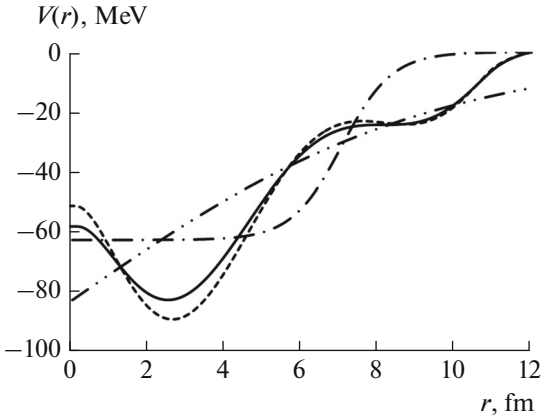

Fig. 5. Potentials fitted to data in Fig. 1b. The $V_F(r)$ potential (solid line), the $V_{RF}(r)$ version including rearrangement (dashed line) and the fitted $V_{FWS}(r)$ potential (double dotted-dashed line) are shown. Also shown is the conventional Woods–Saxon $V_{WS}(r)$ potential (dashed-dotted line).

note that for nonsingular potential V, $\frac{d^2R}{dr^2} = 0$ when $R(\vec{r}) = 0$. As seen from Fig. 2b, this condition is not fulfilled at the nodes of the experimental $R_p^2(r)$. Moreover, in the vicinity of these nodes, the uncertainty in $\Delta\rho_p(r)$ is larger than its value. This leads to a very large uncertainty for V in regions of the nodes. We have thus constructed from the experimental data radial wave functions having a proper behavior at the zeroes (around 2.6 and 4.9 fm), by fitting the experimental point radial wave function to the function $R_p = A\sin(kr + \varphi)$ in the vicinity of the nodes. The corresponding (constant) potentials are shown by the dashed lines in Fig. 3.

In view of the resulting potentials shown in Fig. 3, we have constructed from the experimental data a function $R_p^2(r)$ having a proper behavior at the zeroes (around 2.6 and 4.9 fm). This was done by fitting the experimental point radial wave function to a sum of two separate sine functions $R_p = A\sin(kr + \varphi)$ spliced together at $r \sim 5.3$ fm. This function is shown by the dashed line in in Fig. 4a. Also shown in Fig. 4a are the experimental data (solid line) and the uncertainty (dotted lines). We then determined the nuclear potential from the fitted $R_p^2(r)$ (dashed line of Fig. 4a) by employing Eqs. (7) and (9). The results are shown by the dashed line of Fig. 4b. Note the step function behavior of the resulting potential.

We have therefore considered several nuclear central potentials with parameters obtained by fits of the calculated $R_p^2(r)$ to the corresponding experimental data, taking into account the Coulomb potential, Eq. (14). In Fig. 5 we show the potential $V_F(r)$, solid line, which is a smoothed potential of a jagged, multiply connected linear potential by taking the values of the jagged, linear potential at $r = 3$, 6 and 9 fm as free parameters, the value of the potential at $r = 0$ fm is constrained to reproduce the experimental value of 7.25 MeV for the separation energy of the proton $3s_{1/2}$ orbit and the value of the potential is taken to be 0.0 MeV at $r = 12$ fm. The values of $V_F(r)$ are determined by polynomial fit to all the values of the jagged, linear potential and is smoothed near $r = 0$ and 12 fm so that the first derivative is zero. From a fit to the experimental data of $R_p^2(r)$, solid line in Fig. 2b, we obtained that the values of $V_F(r)$ at $r = 0$, 3, 6, 9 and 12 fm are −58.19, −83.15, −34.50, −23.54 and 0.0 MeV, respectively, with a corresponding $\chi^2/N = 1.15$. Similarly, the potential $V_{RF}(r)$ (dashed line in Fig. 5) is obtained by a fit to $R_{Rp}^2(r)$ (dashed line of Fig. 2b) resulting with the values of −51.32, −88.29, −33.64, −23.96 and 0.0 MeV, for $V_{RF}(r)$ at $r = 0$, 3, 6, 9 and 12 fm respectively, with a corresponding $\chi^2/N = 1.81$. The potential $V_{WSF}(r)$, dashed double dotted line

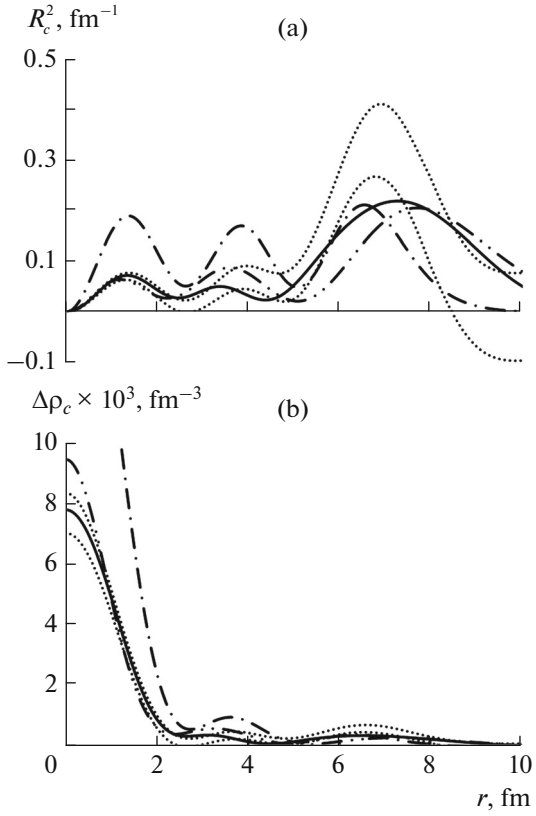

Fig. 6. Experimental values of $R_c^2(r) = 4\pi r^2 \Delta\rho_c(r)$ (a) and $\Delta\rho_c(r)$ (b) plotted between dotted lines of error limits. They are compared to calculated charge distributions due to the $3s_{1/2}$ wave functions of the fitted $V_F(r)$ potential (solid lines), the fitted Woods–Saxon $V_{FWS}(r)$ potential (double dotted-dashed lines) and the conventional $V_{WS}(r)$ potential (dashed-dotted lines).

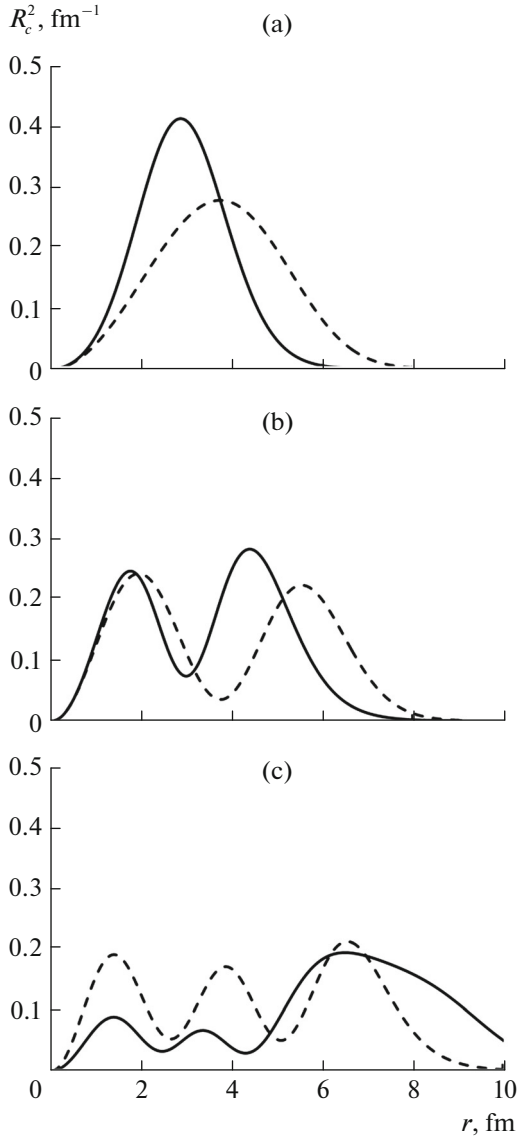

Fig. 7. Calculated squared wave funcitons, $R_c^2(r) = 4\pi r^2 \Delta\rho_c(r)$, of a proton in the $1s_{1/2}$ (a), $2s_{1/2}$ (b) and $3s_{1/2}$ (c) orbits in the $V_F(r)$ potential (solid lines) and the conventional $V_{WS}(r)$ potential (dashed lines).

in Fig. 5, is obtained by fitting experimental data of $R_p^2(r)$ to that calculated using Woods–Saxon potential, Eq. (13), obtaining the values of −167.95 MeV, −0.03 and 4.68 fm for V_0, R_1 and a_0, respectively, with the corresponding value of $\chi^2/N = 3.28$. For comparison, we also show by the dashed-dotted line the Woods–Saxon Potential $V_{WS}(r)$ using the conventional values of −62.712 MeV, 7.087 and 0.65 fm for V_0, R_1 and a_0, respectively, with the corresponding value of $\chi^2/N = 8.85$.

In Figs. 6a, 6b we compare the experimental results of the square of the convoluted (charge) radial wave function $R_c^2(r)$ and the charge density $\Delta\rho_c(r)$ of the proton $3s_{1/2}$ orbit, respectively, with the corresponding results obtained from the potentials shown in Fig. 5. The experimental data is given by the region defined by the dotted lines and the results obtained using, $V_F(r)$, $V_{WSF}(r)$ and $V_{WS}(r)$ are shown by the solid, dashed-double dotted and dashed-dotted curves, respectively. Note that the results of the fitted potentials $V_F(r)$ and $V_{RF}(r)$ are in very good agreement with the experimental data. The results of the fitted potential $V_{WSF}(r)$ are in reasonable agreement with data. It is important to point out that the amplitudes of the oscillations of $R_c^2(r)$ obtained from the conventional WS potential $V_{WS}(r)$ are much larger than those of the experimental data for r smaller than 5.0 fm and much smaller than data for r larger than 5.0 fm. Also, as noted in Refs. [4, 5], the calculated value of the charge density $\Delta\rho_c(r)$ at $r = 0$ fm obtained using the $V_{WS}(r)$ potential is larger than the experimental value [4, 5] by a factor of two.

In Fig. 7a–7c we compare $R_c^2(r)$, the square of the radial functions, of the $1s_{1/2}$, $2s_{1/2}$, and $3s_{1/2}$ proton

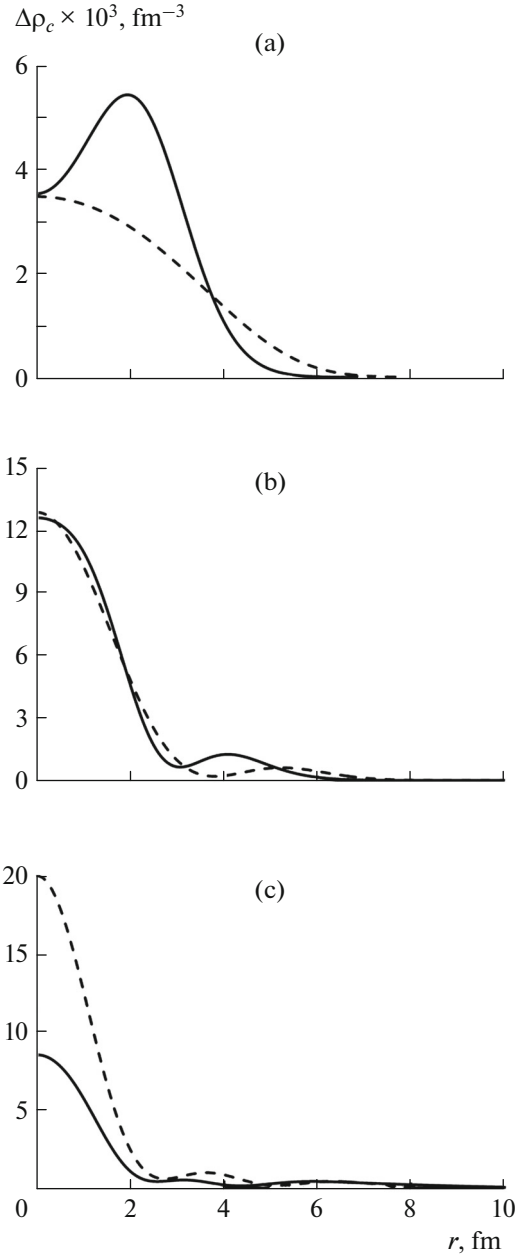

Fig. 8. Calculated charge densities of a proton in the $1s_{1/2}$ (a), $2s_{1/2}$ (b) and $3s_{1/2}$ (c) orbits in the $V_F(r)$ potential (solid lines) and the conventional $V_{WS}(r)$ potential (dashed lines).

orbits, respectively, obtained from the fitted potential $V_F(r)$ (solid lines) with those obtained from the conventional WS potential $V_{WS}(r)$ (dashed-double dotted lines). The separation energies of the $1s_{1/2}$, $2s_{1/2}$, and $3s_{1/2}$ proton orbits are −47.09, −22.64 and −7.24 MeV and −36.31, −24.46 and −8.00 MeV for the $V_F(r)$ and $V_{WS}(r)$ potentials, respectively. Note the relatively large separation energy of the $1s_{1/2}$ proton orbit obtained for the $V_F(r)$, which is closer to the experimental data [12].

In Fig. 8a–8c, we show the corresponding charge density of the $1s_{1/2}$, $2s_{1/2}$, and $3s_{1/2}$ proton orbits for the $V_F(r)$ (solid lines) and $V_{WS}(r)$ (dashed-double dot lines) potentials, respectively. We point out that at $r =$ 0 fm only the proton s orbits contribute to the charge density, $\rho_c(r)$, in ^{206}Pb. The calculated value of $\rho_c(0) = 0.060$ fm^{-3} for the fitted potential $V_F(r)$ is significantly smaller than the value of $\rho_c(0) = 0.073$ fm^{-3} for conventional Woods–Saxon $V_{WS}(r)$, in good agreement with experimental value of $\rho_c(0) = 0.063$ fm^{-3} [4, 5].

3. CONCLUSIONS

Starting from the single particle Schroedinger equation for the function $\Psi(\vec{r})$, with eigen-energy E, we have derived a novel method for determining the corresponding single particle potential V from $[\Psi(\vec{r})]^b$, where b is a real number, assuming that $[\Psi(\vec{r})]^b$, $\vec{\nabla}\Psi$ and $\Delta[\Psi(\vec{r})]^b$ are known for all positions$(\vec{r})$, see Eqs. (2) and (3). It is clear from the Schroedinger equation that for a nonsingular V, $\vec{\nabla}\Psi(\vec{r}) = 0$ when $\Psi(\vec{r}) = 0$. This condition is extended to the requirements that for $b > 2$, $\vec{\nabla}[\Psi(\vec{r})]^b = 0$ and $\Delta[\Psi(\vec{r})]^b = 0$ when $[\Psi(\vec{r})]^b = 0$. For $b = 2$, we have from Eqs. (2) and (3) that the potential $V(\vec{r})$ is given in term of the corresponding single particle matter density $\rho(\vec{r})$ (for real $\Psi(\vec{r})$) and its first and second derivatives.

We have presented results for the nuclear single particle potential V associated with the proton $3s_{1/2}$ orbit in ^{206}Pb deduced from the electron scattering [4, 5] data for the charge density difference between the isotones ^{206}Pb – ^{205}Tl, obtained by employing our new method for the special case of spherical symmetry, Eqs. (7) and (10). The results for the proton $3s_{1/2}$ orbit in ^{206}Pb, shown in Fig. 3a, exhibit large uncertainty for V around the zero values of the $3s_{1/2}$ proton density $\Delta\rho_p(r)$, where the experimental uncertainty in $\Delta\rho_p(r)$ is lager than its value. It is difficult to see whether the conditions that the first derivative of $\Delta\rho_p(r)$ and the corresponding expression in the square brackets in the right hand side of Eq. (10) vanish when $\Delta\rho_p(r) = 0$, which are necessary for determining a nonsingular V, are satisfied by the experimental data for $\Delta\rho_p(r)$.

We have also carried out a least-square fit of the calculated density $\Delta\rho_p(r)$ of the $3s_{1/2}$ point proton density to the corresponding experimental data, using

the three parameters Woods–Saxon potential and a potential defined by its values at $r = 0$, 3, 6, 9, and 12 fm and compared with the results obtained from the conventional Woods–Saxon potential. We note that the fitted potentials exhibit large diffuseness (Fig. 5). As seen from Fig. 6, we obtained good agreements with the experimental data for the fitted potentials, whereas the results obtained from the conventional Woods–Saxon potential are in disagreement with data. Clearly more accurate experimental data for $\Delta\rho_p(r)$ with uncertainty smaller by a factor of two or more may help in answering the question how well can the data be reproduced by a calculated $3s_{1/2}$ single particle wave function and thereby determining the form of V.

ACKNOWLEDGMENTS

The authors would like to thank Professor I. Talmi for suggesting the problem and for many discussions. S. Shlomo thanks The Weizmann Institute of Science for the kind hospitality. This work was supported in part by US Department of Energy under Grant no. DOE-FG03-93ER40773.

REFERENCES

1. De Shalit, A. and Talmi, I., *Nuclear Shell Model*, New York: Academic, 1963.
2. Bohr, A. and Mottelson, B.R., *Nuclear Structure*, New York: Benjamin, 1975, vol. 2.
3. Agrawal, B.K., Shlomo, S., and Kim Au, V., *Phys. Rev. C*, 2005, vol. 72, p. 014310.
4. Cavedon, J.M., et al., *Phys. Rev. Lett.*, 1982, vol. 49, p. 978.
5. Frois, B., et al., *Nucl. Phys. A*, 1983, vol. 396, p. 409.
6. Pandharipande, V.R., Sick, I., and deWitt Huberts, P.K.A., *Rev. Mod. Phys.*, 1997, vol. 69, p. 981.
7. Shlomo, S., in *The Universe Evolution: Astrophysical and Nuclear Aspects*, Blokhintsev, L. and Strakovsky, I., Eds., Nova Sci., 2013, p. 323.
8. Anders, M.R., Shlomo, S., and Talmi, I., arXiv:1504.05507 [nucl-th].
9. Shlomo, S., Anders, M.R., and Talmi, I., *J. Phys.: Conf. Ser.*, 2015, vol. 633, p. 012028.
10. Elton, L.R.B., *Nuclear Sizes*, London: Oxford Univ. Press, 1961.
11. Euteneuer, H., Friedrich, J., and Voegler, N., *Nucl. Phys. A*, 1978, vol. 298, p. 452.
12. Vorobev, A.A., Dotsenko, Y.V., Lobodenko, A.A., Miklukho, O.V., Tkach, I.I., Tsaregorodtsev, A.Y., and Shcheglov, Y.A., *Phys. At. Nucl.*, 1995, vol. 58, p. 1817.